SAND2015-4284C

Modal Decomposition of Pressure Data in Cavity Flows

Katya M. Casper*and Srinivasan Arunajatesan†
Sandia National Laboratories, Albuquerque, NM 87185

The flow over aircraft bays exhibits many characteristics of cavity flows, namely resonant pressures that can create high structural loading. An extensive dataset within both simple and complex cavities was previously obtained and analyzed using power-spectral densities, coherence levels, and cross correlations between sensor pairs within the cavity. More in-depth analysis of the flow structure is studied here using modal decomposition techniques. Both Proper Orthogonal Decomposition (POD) and Dynamic Mode Decomposition (DMD) were applied to the experimental and computational results within a simple rectangular cavity. POD was able to show that the cavity modes are coherent across the cavity width. Only higher modes that were associated with more turbulent fluctuations in the cavity exhibited spanwise variations. DMD was able to isolate structures associated with single frequencies in the flow. Coherent structures across the cavity width were again found at the cavity tones. However, additional DMD modes in between the dominant frequencies also appeared. Many of these additional modes had similar structures to the cavity tones mode shapes. These additional modes were associated with a low-frequency modulation of the cavity tones. POD analyses was than applied to a complex cavity. POD mode shapes exhibited similar structures to the simple rectangular cavity; however, the energy was more distributed among the many modes. This reflected the more complex flowfield in the cavity. Future analyses will apply POD and DMD to computations of the complex flowfield, to better understand its three-dimensional structure.

Nomenclature

D	cavity depth (mm)	q_∞	freestream dynamic pressure (kPa)
f	frequency (kHz)	Re	freestream unit Reynolds number (1/m)
L	cavity length (mm)	U_∞	freestream velocity (m/s)
M	freestream Mach number	W	cavity width (mm)
P_0	total pressure (kPa)		

I. Introduction

The flow over aircraft bays can generate significant structural loading caused by resonant pressure fluctuations created in the bay. This resonance is typical of cavity flows, which have been extensively studied over the years.[1,2] The flow over a cavity can set up a feedback loop between the free shear layer and the cavity's acoustic field that creates resonant tones or 'Rossiter' modes in the cavity.[3] This typically occurs in 'open' subsonic cavity flows when the cavity length-to-depth ratio L/D is less than about 6-8.[4] The amplitude of the modes can be quite large, and sound pressure levels (SPL) greater than 170 dB have been reported.[5] The frequencies of these modes in compressible flow can be estimated using Heller and Bliss's semi-empirical method.[6] However, the distribution of the mode amplitudes and their frequencies varies greatly depending on flow condition and cavity geometry.

*Senior Member of the Technical Staff, Engineering Sciences Center, Member AIAA, kmcaspe@sandia.gov, (505) 844-1574
†Principal Member of the Technical Staff, Engineering Sciences Center, Senior Member AIAA

Sandia National Laboratories is a multi-program laboratory managed and operated by Sandia Corporation, a wholly owned subsidiary of Lockheed Martin Corporation, for the U.S. Department of Energy's National Nuclear Security Administration under contract DE-AC04-94AL85000.

Previous experiments in rectangular cavities of various width and depth have been conducted to study the unsteady fluctuations and their coupling to store vibration.[7,8] Velocimetry measurements of a rectangular cavity in supersonic flow have shown that the cavity width alters the flow field structure.[9] However, there are limitations when applying this work to actual aircraft bays, which have many complex features that are not captured by a simple rectangular cavity geometry.[10]

Limited work has been done to explore complex configurational differences[10–14] and much of this work has focused on the control of pressure fluctuations in these complex geometries, not on understanding the differences from simple geometries. To address this shortcoming, a complex cavity geometry was designed and fabricated for wind tunnel testing that allows features representing a realistic aircraft-bay geometry to be incorporated one by one. A parametric study of these geometric features including shaped inlets, internal cavity variations, and doors was conducted in both subsonic and supersonic flow to isolate important parameters for the pressure loading in aircraft bays and to investigate the limits of rectangular cavities in representing flight geometry.[15,16] Pressure measurements were obtained along the cavity centerline, and across the front, middle, and rear span of the cavity. The analysis of this pressure data focused on power spectral densities and cross-coherence and cross-correlation analyses between sensor pairs.

This analysis provided valuable insight into the effect of the complex configurations on cavity pressures. However, more advanced analyses can help better understand the differences between the flow structures in each configuration. Modal decomposition techniques including Proper Orthogonal Decomposition (POD)[17] and Dynamic Mode Decomposition (DMD)[18] are used here to explore the complex flowfields. These techniques have traditionally been applied to flowfield velocity measurements obtained from Particle Image Velocimetry (PIV) or computations. The technique allows the complex flowfield to be decomposed into coherent structures. POD ranks the structures by their energy content, while DMD tends to identify structures that have dynamics which last over time.[18]

Other researchers have conducted such modal decompositions on cavity flows.[18–21] In contrast to these papers which typically studied flowfield results, here, we look at pressure data on the floor of the cavity to being to understand how the flowfield is coupling to the surface pressure. In the present work, these techniques are initially applied to the experimental pressure data obtained in a simple rectangular and complex cavity. This application is somewhat different than traditional applications: instead of applying the techniques to a dense spatial grid with a limited amount of snapshots in time, coarse lines of pressure sensors in the cavity bay were used, but with a large number of data samples in time. Spatial resolution limitations, particularly for DMD, requires further study using computational datasets. These provide much better spatial resolution, though over a more limited time interval.

II. Experimental Setup

II.A. Sandia Trisonic Wind Tunnel

Experiments are performed in Sandia's Trisonic Wind Tunnel (TWT). This is a blowdown-to-atmosphere facility using air as the test gas. The full test section is 305×305 mm and is enclosed in a pressurized plenum. Fig. 1 shows the cavity installed on the top wall of the test section for subsonic tests. Recent work has identified an optimal wall configuration incorporating acoustic dampening to reduce tunnel mode interference with the cavity flows.[22] The present results uses this optimal configuration. A porous floor insert and one porous sidewall helps ensure that tunnel modes are dramatically reduced from a solid wall configuration.

Typical run conditions are given in Table 1. The Mach number is computed from a centerline static pressure measurement 21.9 cm upstream of the cavity leading edge. The incoming boundary layer to the cavity is fully turbulent. Previous (unpublished) measurements have shown that the boundary layer thickness at the cavity leading edge is about 0.3–0.4 D. The stagnation temperature is held constant at $321 \pm 2K$. The walls of the test section remain near room temperature at $307 \pm 3K$.

Table 1. Typical run conditions.

M_∞	q_∞ (kPa)	P_0 (kPa)	$Re \times 10^6/m$
0.8	33	112	13

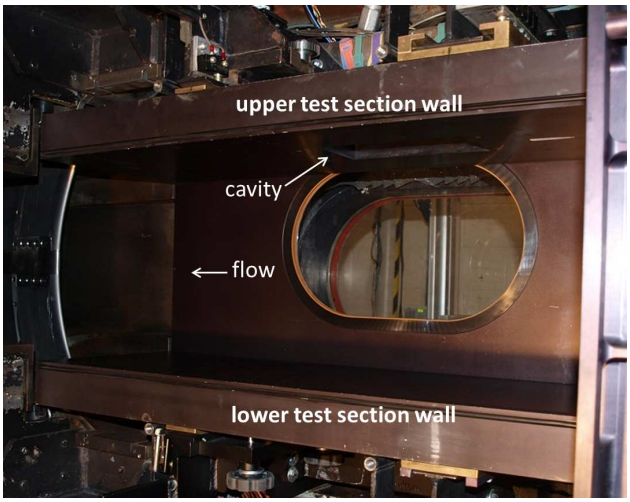

Figure 1. Complex cavity installed in the TWT subsonic full nozzle.

II.B. Cavity design and apparatus

The complex cavity apparatus is built up from a simple rectangular cutout that is integrated into a tunnel wall insert (Fig. 2(a)). This cavity has a length, width, and depth of 203, 102, and 29 mm, respectively. The L/D ratio of 7 categorizes this simple cavity flow at the upper limit of 'open' in subsonic flows.[4] To create distinct complex geometric configurations, different pieces can be added to the front and sides of the rectangular cavity. The basic sensor layout and coordinate system remains the same in the complex geometry. The complex geometry is described in depth in Refs. 15 and 16. Fig. 2(b) shows the configuration that is analyzed in the present paper. This configuration has a centered scoop and tooth at the leading edge, two open doors, and a side insert.

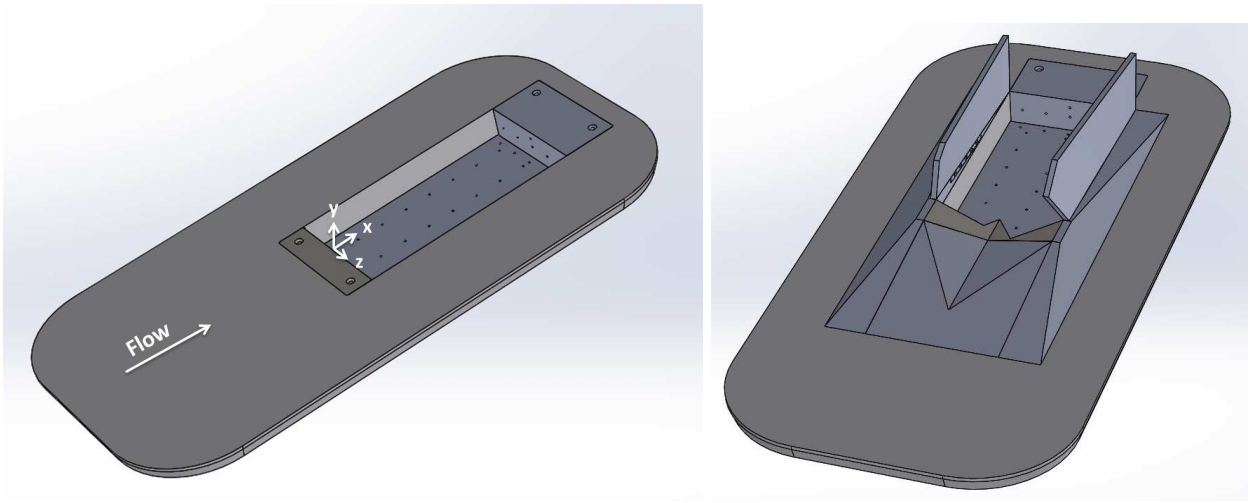

(a) (b)

Figure 2. Cavity tunnel insert (a) simple rectangular cavity; (b) complex cavity with centered scoop and tooth, two open doors, and a side insert.

II.C. Instrumentation and Data Acquisition

The complex geometry has forty positions available for pressure measurements, thirty of which were used during testing. Five sensors are located in the spanwise direction along the forward floor of the cavity (FFP1–5, Fig. 3(a)). There is also a line of sensors down the center of the cavity (C2-C7). Two sensors are located on either side of sensor C4 in the spanwise direction and are designated L4 and R4. There is another spanwise line of sensors at the rear of the cavity (RFP1–5), as well as at the aft wall of the cavity (AWP1–5, Fig. 3(b)). A final sensor AWP6 is located on the cavity centerline, on the aft wall above sensor AWP3. A schematic of these locations with respect to the cavity geometry is shown in Fig. 3(c). When the centered tooth is installed, the front floor sensors FFP1-5 are located beneath an overhang created by the tooth. Sensor C2 is just downstream of the tooth on the cavity floor. When the side insert is installed, sensor R4 is located in front of the insert, while sensors RFP5 and AWP5 are covered.

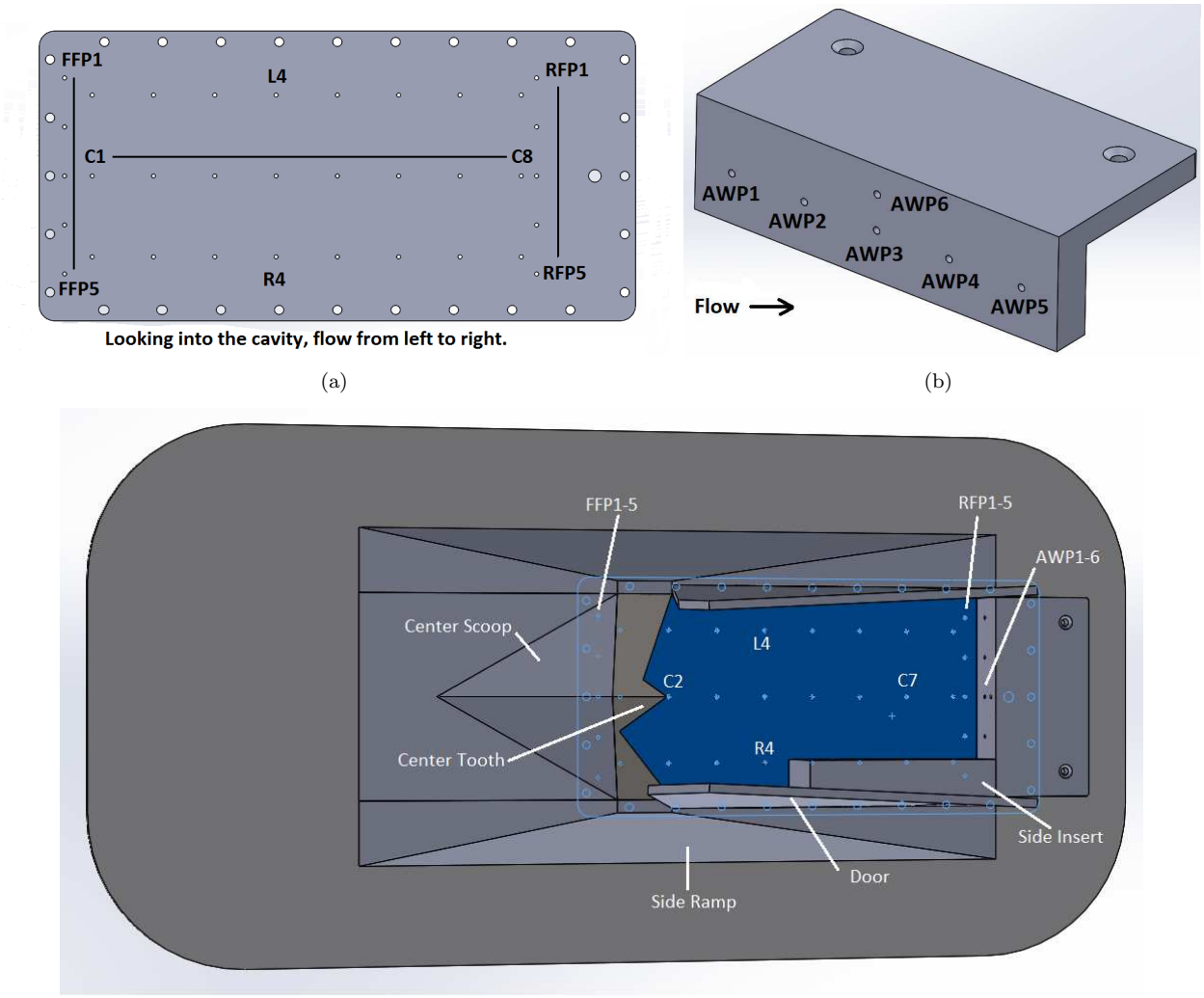

Figure 3. Complex cavity sensor locations (a) Floor plate; (b) Aft cavity wall; (c) Floor plate and aft cavity wall installed in complex geometry.

Kulite XCQ-062-30A (or similar) pressure transducers are used to measure the unsteady cavity pressure fluctuations. These sensors have a resonant frequency of 240–300 kHz. The repeatability is approximately 0.1% of the full scale. The Kulite signal output is passed through an Endevco Model 136 DC Amplifier. This provides a 10 V excitation and is also used to supply a gain of 50–100. A Krohn-Hite Model 3384 Tunable Active Filter is used to provide a 50 kHz anti-aliasing low-pass Bessel filter. This filter has eight poles and provides 48 dB attenuation per octave. The Kulite sampling frequency is typically 500 kHz. Data are acquired using a National Instruments PXI-1042 chassis with 14-bit PXI-6133 modules (10 MHz bandwidth).

III. Computational Setup

The flow simulations for the complex cavities are performed using the SIGMA CFD code, a multi-block, structured grid, finite volume solver for compressible flow. The finite volume method is formally second order, but employs expanded, directionally-split, stencils for constructing the inviscid fluxes, resulting in improved accuracy over standard second order finite volume discretizations. The inviscid flux scheme is a hybrid centered/dissipative scheme, consisting of the sum of a non-dissipative centered flux approximation and a mixed 2nd/5th order dissipative flux that is weighted using a flow sensor to avoid excessive numerical dissipation in regions of resolved turbulent flow (i.e., LES regions). Details of the numerical method can be found in Arunajatesan et. al.[23] and Barone and Arunajatesan.[24] The simulations employ a hybrid RANS/LES turbulence model, where turbulent flow near the walls is modeled using a k-epsilon RANS model, while further from solid walls the model transitions to LES. Complete details of the simulations, boundary conditions and meshes etc. are given in Barone et. al.[25] The wall pressures used in the analysis here are collected at specified locations during the simulations, by sub-sampling the data every 20 time steps (every 10 μs).

IV. Modal Decomposition Techniques and Joint Time Frequency Analysis

Two modal decomposition techniques are applied to the complex cavity flow datasets. A summary of the different techniques and some of their limitations can be found in Ref. 26. Proper Orthogonal Decomposition (POD)[17,27] is initially applied to this data set. The decomposition is done using a singular value decomposition of the data set. From the POD analysis, spatial mode shapes are obtained as well as mode amplitude coefficient variations in time. In order to look at the dynamic content of the spatial modes, power spectral densities (PSD's) of the mode amplitude coefficients are also computed.

POD ranks structures by their energy content. Because of this ranking, it was found that the local mean pressure at each sensor location must be subtracted prior to computing the POD. Also, the pressure data at each sensor location was normalized by the local RMS pressure. This allows data over different parts of the cavity to be compared. Without this normalization, data at the aft end of the cavity dominates the results because the RMS pressure at the aft end of the cavity is significantly higher than the front of the cavity.

One drawback of the POD method is that it cannot identify structures attached to a single frequency; each mode shape can involve multiple frequencies. To be able to identify flow structures associated with a single frequency, Dynamic Mode Decomposition (DMD)[18] is also applied to this dataset. DMD identifies structures with dynamics that last over time. For computational speed, a streaming DMD method is used as described in Ref. 28. Dominant frequencies are obtained from the eigenvalues of the DMD decomposition. Mode amplitudes are obtained from the norm of the DMD modes. In order to determine which modes are contributing to the system dynamics, the DMD mode norms are additionally scaled using λ^m, where λ is the eigenvalue and m is the DMD mode number.[26] Only modes with a normalized amplitude above 0.002 are considered.

Joint-time frequency analysis of the pressure traces is also conducted using a wavelet transform. This technique shows the frequency content in the cavity as a function of time, and has been used in other unsteady applications such as wake transition, meteorological studies, and cavity flows.[29–32] The transform provides good time resolution for identifying mode switching in the cavity. However, it has poor frequency resolution compared to alternate joint time-frequency methods such as the short-time-Fourier transform. The transform is computed using Matlab software from Ref. 31. A Morelet mother wavelet is used.

V. Results

V.A. Simple rectangular cavity

V.A.1. Proper Orthogonal Decomposition

POD analysis is first applied to the experimental data in the simple rectangular cavity (Fig. 2(a)). The analysis was applied to three lines of sensors, one across the front span of the cavity (FFP1–5), one along the cavity centerline (FFP3, C2–C7, AWP3), and one across the aft wall of the cavity (AWP1–5). Fig. 4 shows PSD's of the measured pressures across the front of the cavity, and at several locations along the cavity centerline. The Rossiter modes are clearly evident as strong peaks in the power spectra and are marked with

dashed grey lines. There is little variation in the frequency content or amplitude of pressure fluctuations across the front span of the cavity. However, both the mode amplitudes and broadband pressure fluctuations increase in amplitude with downstream distance. More details about these measurements can be found in Refs. 15 and 16.

Fig. 6(a) shows the mode shapes computed from sensors FFP1–5. The first mode is constant across the cavity, while higher modes have sinusoidal variations across the cavity width. Fig. 6(b) shows the PSD's of the mode amplitude coefficients. This shows what frequency content in the overall PSD's contributes to each mode shape. The amplitude of the model coefficient PSD's are not the same as the PSD's of the full pressure signal. This is because the mode shape amplitudes are less than unity and the pressure matrix has been normalized by the local RMS pressure. The results show that for the front span of the rectangular cavity, the Rossiter modes contribute to the first POD mode, but not to the higher modes. Since the first mode has a flat amplitude distribution across the cavity, this indicates that the Rossiter modes are almost completely coherent across the front of the cavity. This result is substantiated by looking at the energy distribution among the modes (Fig. 5). The POD will always calculate the same number of modes as the quantity of sensors used in the computation. However, these modes may not all be physically relevant. For example, at the front of the cavity, the first mode contains 50% of the total energy. The remaining modes have much lower contributions to the overall energy, of 20% or less. This shows that the first mode dominates the results, again indicating that the flow is coherent across the cavity width. The remaining energy is broadband and does not appear to be tied to any particular Rossiter mode or other resonant peak in the pressure spectra.

POD is also applied to a line of eight sensors along the cavity centerline (Fig. 7). The computed mode shapes correspond to different standing wave patterns in the cavity. The corresponding PSD's of the mode amplitude coefficients show that the Rossiter mode frequencies appear in all of these modes, but there is a gradual shift from all Rossiter frequencies contributing to the first POD mode, to only higher frequency Rossiter modes contributing to the higher POD modes. For example, the first Rossiter mode is dominant in the first POD mode. However, the amplitude of that frequency decreases for higher POD modes. Similarly, the second Rossiter mode has a high amplitude in the first three POD modes and then decreases for higher POD modes. The distribution of energy among the POD modes shows a different behavior than the front of the cavity (Fig. 5). Here, the energy is more evenly distributed among the various mode shapes, which agrees with the Rossiter modes contributing to many of the POD modes.

POD was also applied to a line of sensors across the aft cavity wall. The mode shapes are similar to the front cavity span and are not shown, however, the distribution of energy is more evenly distributed across the modes as shown in Fig. 5. This indicates that the aft cavity wall pressure signals contain more broadband turbulent fluctuations, which leads to more energy in the higher POD modes.

The limited spatial resolution of the experimental pressure measurements prevents looking a flow structures throughout the cavity. As a result, POD is applied to computations of the simple rectangular cavity. Pressure traces were extracted from a grid of locations on the cavity floor as described in Section III. A 21×21 grid was found to provide sufficient spatial resolution for the analysis; results did not change for grids of 41×41 or 81×81 locations. However, a finer grid of 81×81 sensors are used for the subsequent analysis.

Many more POD modes are obtained from the computational results because of the larger number of sensors. However, the first 6 POD modes again contain the majority of the energy. The PSD's of the modal amplitude coefficients again show that the modes are related to a broad range of frequencies. The first 4 modes contain most of the cavity tonal content. Higher modes are associated with the broadband frequency content in the cavity, similar to the experimental POD results.

The much denser spatial grid of sensors in the computational results allows a contour plot of POD mode shapes (Fig. 8). Modes that extend across the span of the cavity are obtained for the first 4 mode shapes. This result is consistent with the PSD's that show that these modes are associated with the resonant cavity tones. Higher modes above 5 then begin to exhibit spanwise variations, consistent with the broadband frequency content seen in the PSD's for these modes.

V.A.2. Dynamic Mode Decomposition

Because POD could not identify structures associated with a single frequency, DMD was attempted on the experimental results. Unfortunately, the sparse quantity of experimental sensors prevented adequate spatial resolution to capture the cavity dynamics. Results were obtained with non-physical frequencies of cavity

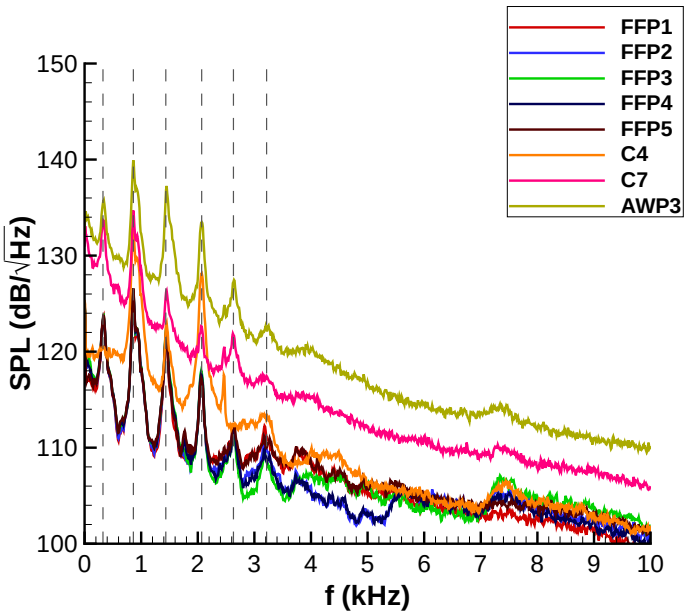

Figure 4. PSD of simple rectangular cavity measurements across the front of the cavity and select locations along the centerline.

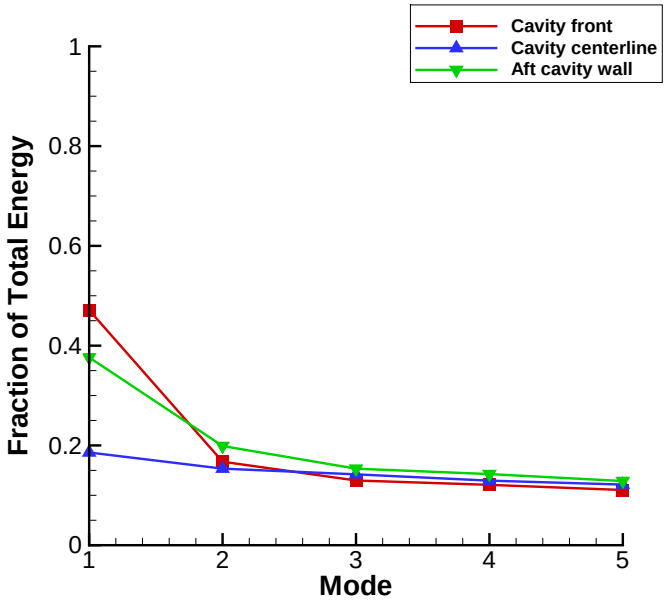

Figure 5. Energy distribution among POD modes in simple rectangular cavity.

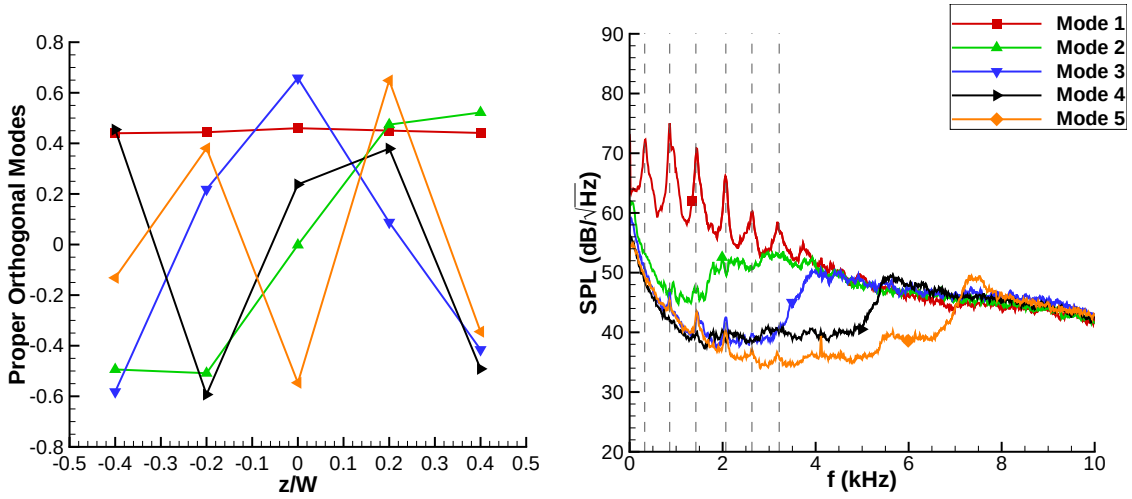

(a) (b)

Figure 6. Simple rectangular cavity front POD modes (a) Mode shapes; (b) PSD of mode amplitude coefficients.

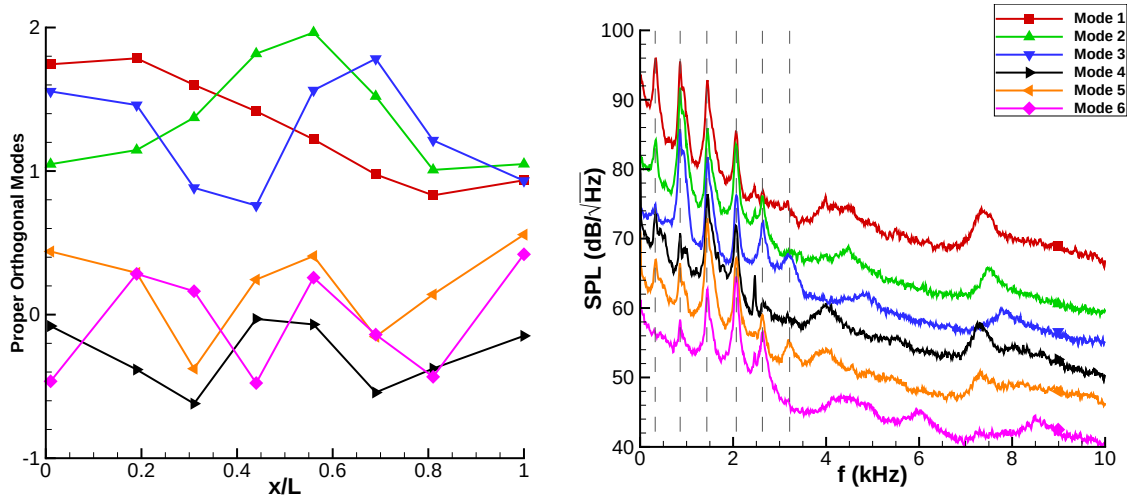

(a) (b)

Figure 7. Simple rectangular cavity centerline POD modes (a) Mode shapes, modes 1 to 3 are shifted upwards for clarity; (b) PSD of mode amplitude coefficients, each mode is offset.

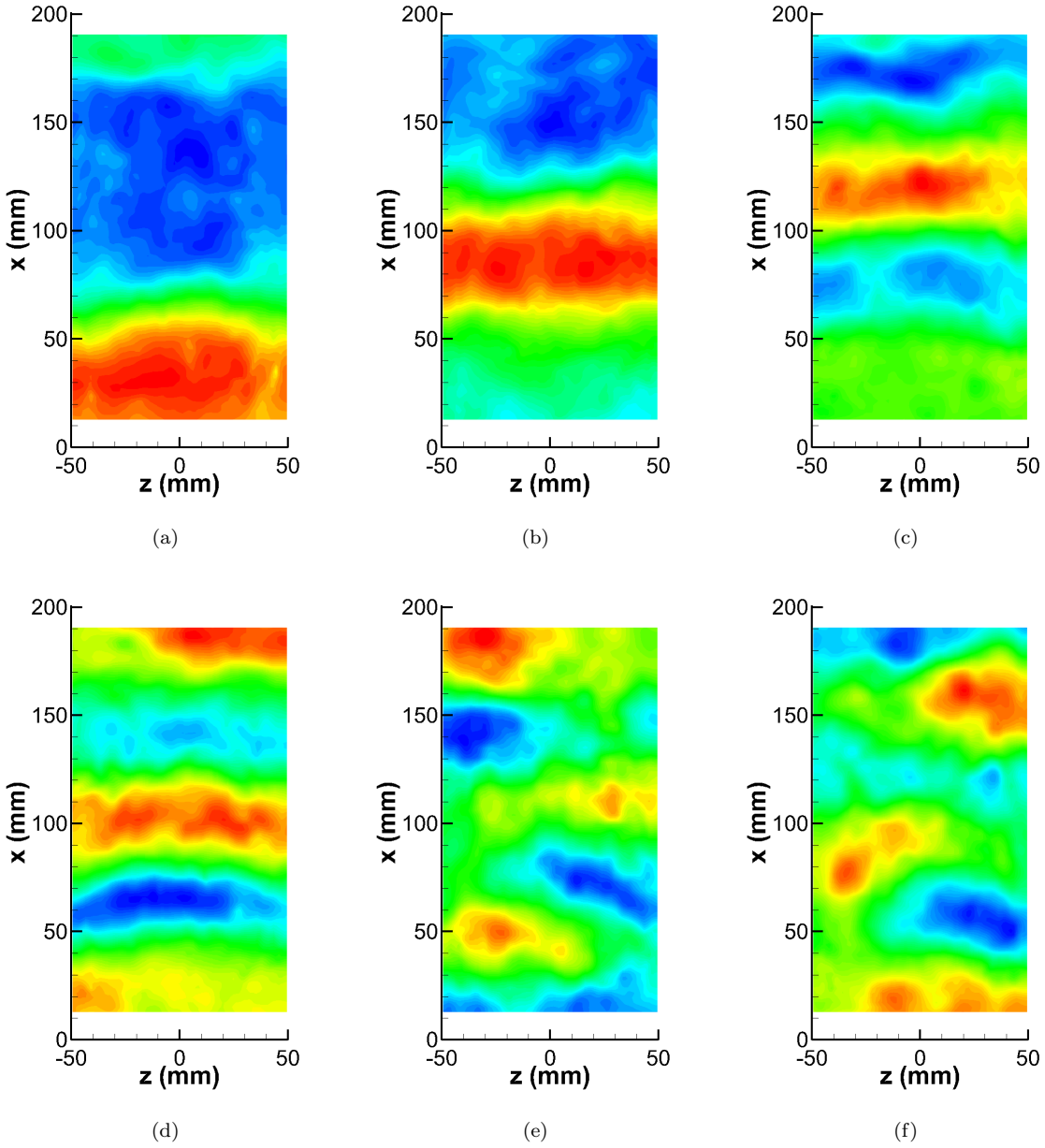

Figure 8. POD of simple rectangular cavity computations at Mach 0.8, mode shapes (a) Mode 1; (b) Mode 2; (c) Mode 3; (d) Mode 4; (e) Mode 5; (f) Mode 6.

fluctuations. DMD, however, could be applied to the computational data. Fig. 9 shows the frequencies of the computed DMD modes with the highest normalized amplitudes. Cavity modes are again marked with dashed gray lines. DMD modes that correspond to each of these cavity tones are obtained; however, there are also additional DMD modes that show up in between the cavity tones.

DMD mode shapes corresponding to the dominant DMD modes are shown in Fig. 10. Mode shapes that correspond to cavity tones are found in Figs. 10(b), 10(f), 10(h), 10(j), and 10(k). These modes all show coherent structures across the cavity span, similar to the POD mode shapes. Higher frequency cavity tones show more defined spanwise strucutures, likely because the short computational time interval does not provide sufficient statistics to clearly respolve the low-frequency content. Modes shapes corresponding to the intermediate frequencies tend to look similar to the nearest cavity tone mode shapes. For example, the DMD mode shape associated with the first cavity tone at 329 Hz (Fig. 10(b)) looks very similar to the DMD mode at 434 Hz (Fig. 10(c)).

One possibility for the grouping of DMD modes around the cavity tones is that the tones are being modulated at a low frequency. To look at this potential modulation further, a joint-time frequency analysis of the computational results was performed to look at the frequency content of the computational results with time. Fig. 11 shows the result of the wavelet transform applied to a pressure trace at FFP3. Mode switching between the different cavity tones can be clearly seen, but there also appears to be a low frequency modulation of some of the tones, particularly at low freuqnecy. Both the DMD and JTF analyses allow this dynamic behavior to be captured, while it was masked within the POD analysis and trditional time-averaged techniques such as PSD's.

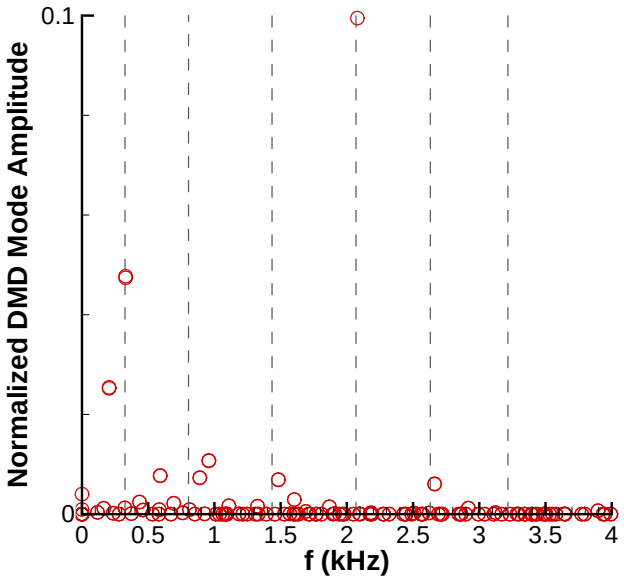

Figure 9. DMD of simple rectangular cavity computations at Mach 0.8, mode frequencies.

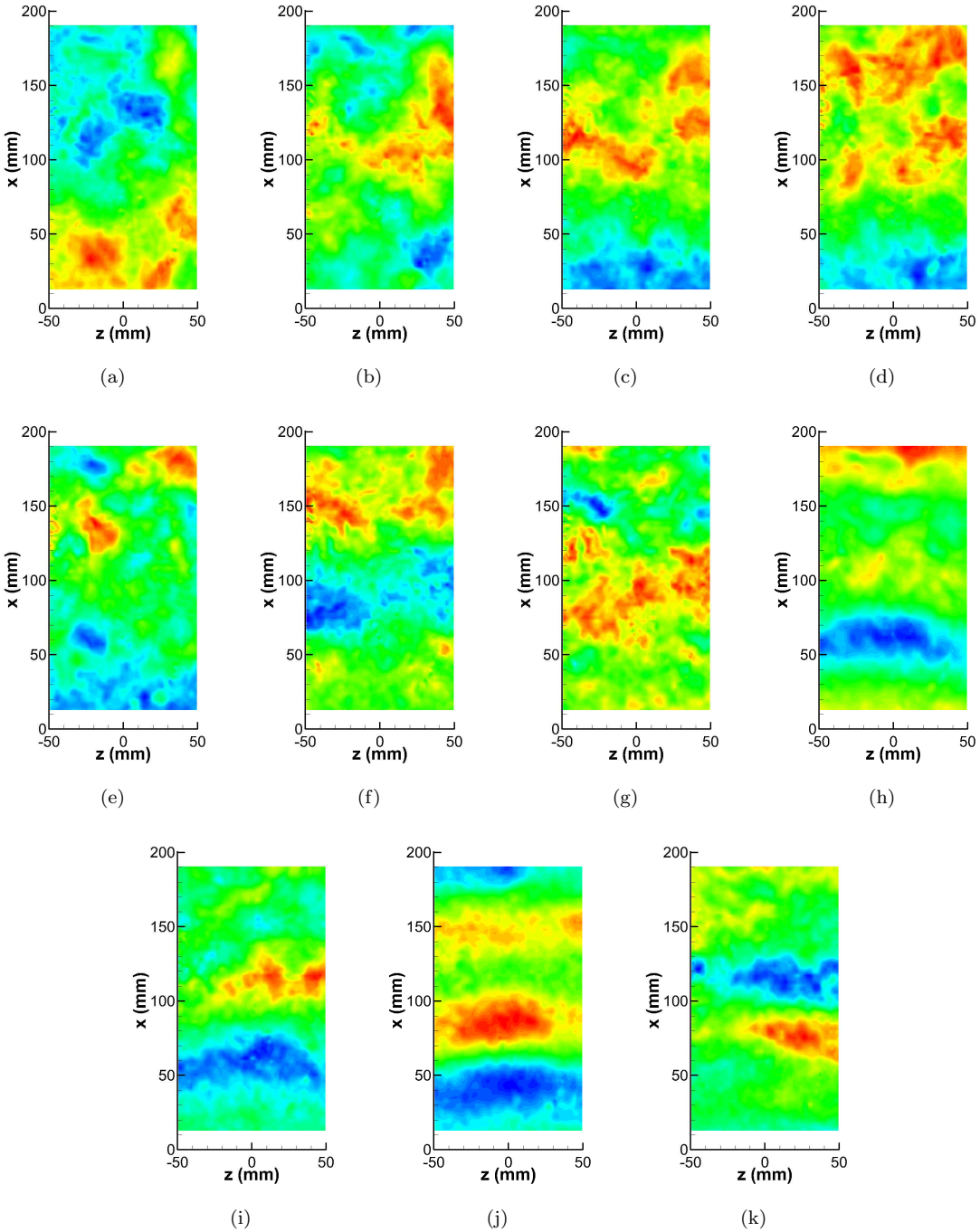

Figure 10. DMD of simple rectangular cavity computations at Mach 0.8, mode shapes (a) f = 205 Hz; (b) f = 329 Hz; (c) f = 434 Hz; (d) f = 590 Hz; (e) f = 693 Hz; (f) f = 890 Hz; (g) f = 958 Hz; (h) f = 1.482 kHz; (i) f = 1.603 kHz; (j) f = 2.080 kHz; (k) f = 2.663 kHz.

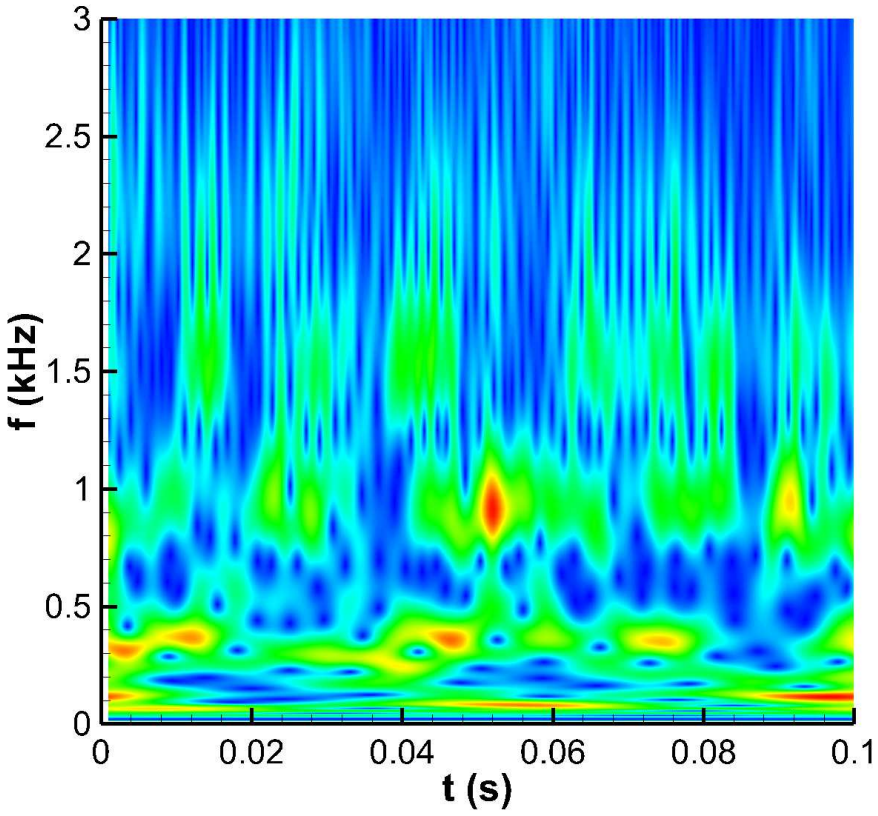

Figure 11. Wavelet transform of simple rectangular cavity computations at FFP3.

V.B. Complex cavity

POD is also applied to the experimental data from the complex configuration (Fig. 2(b)). Fig. 12 shows the PSD's of the measured pressure fluctuations in the cavity. The spectra look quite different from the simple rectangular cavity results shown in Fig. 4. The spectra have larger variations across the front of the cavity. Also, the overall levels of fluctuations in the cavity are higher, particularly at the aft end of the cavity where the spectra have much higher levels of broadband fluctuations.

Results of the POD analysis applied to the front row of sensors are shown in Fig. 13. The POD mode shapes are quite similar to the simple cavity, though some of the signs of the modes are inverted. However, the PSD's of the POD mode amplitude coefficients show some differences. Instead of all the modal content being contained within the first POD mode, there is higher frequency content for all the POD modes. For example, modes 2 and 3 show up in several of the POD modes. This indicates that the cavity modes are less coherent across the cavity width for the complex configuration.

Along the center of the cavity, the mode shapes are again similar to the simple rectangular cavity for the first four modes (Fig. 14). Once again, the first Rossiter mode has a higher amplitude in the first POD mode, but then decreases for higher POD modes. However, higher POD modes lose almost all their Rossiter mode content and are dominated by broadband frequency components. These higher modes also have different shapes than the corresponding rectangular cavity modes, pointing to a different flowfield structure for the complex cavity.

It will be instructive to complete the POD and DMD analyses on computational results for the complex cavity, to identify differences in the flow structure that show up in the cavity floor pressure field. Computations are ongoing, and future work will incorporate this analysis.

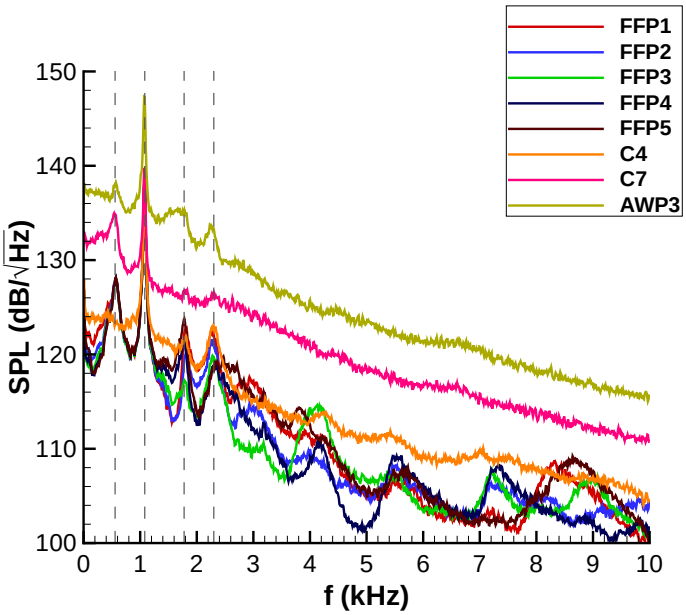

Figure 12. PSD of complex cavity measurements across the front of the cavity and select locations along the centerline.

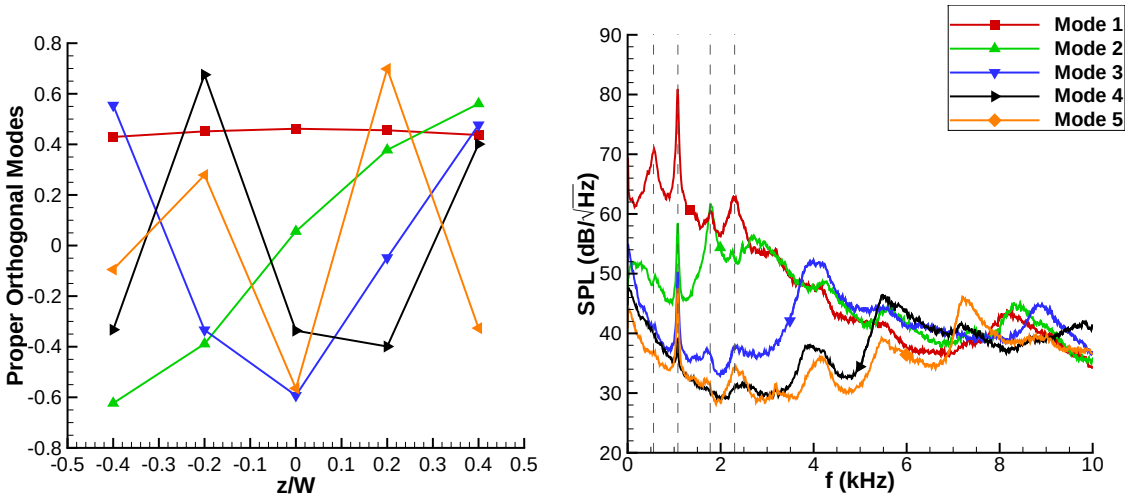

(a) (b)

Figure 13. Complex cavity front POD modes (a) Mode shapes; (b) PSD of mode amplitude coefficients.

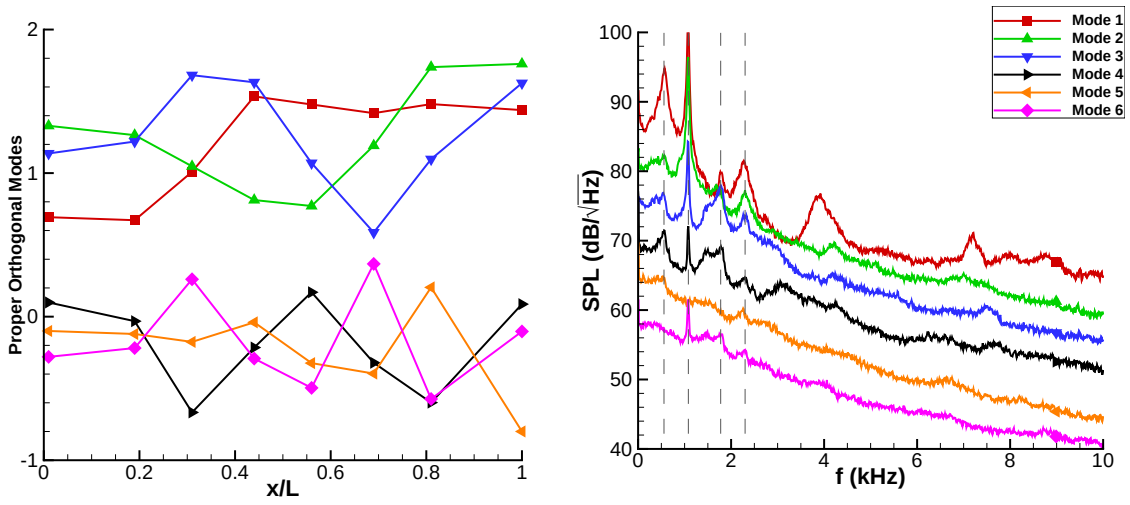

(a) (b)

Figure 14. Complex cavity centerline POD modes (a) Mode shapes, modes 1 to 3 are shifted upwards for clarity; (b) PSD of mode amplitude coefficients, each mode is offset.

VI. Concluding Remarks

Modal decomposition analyses were applied to pressure data within complex cavity flows, to better understand the three-dimensional flow structure. POD analysis was applied to both experimental and computational results within a simple rectangular cavity. These results showed that the flow was coherent across the span of the cavity. Only higher modes showed spanwise variations which corresponded to more turbulent fluctuations in the cavity.

One drawback of POD is that the mode shapes correspond to multiple frequencies in the flow. DMD analysis was applied to isolate flow structures associated with single frequencies. The limited spatial resolution of the experimental sensors prevented using this technique on the experimental data. However, computational results showed the flow structures associated with isolated frequencies. DMD modes corresponding to the cavity tones showed spanwise coherence. Other intermediate frequencies also appeared, many of which had similar mode shapes to the cavity tones. These intermediate frequencies appeared to be associated with a low frequency modulation of the cavity tones, which also showed up in a joint-time-frequency analysis of the pressure data.

POD analysis was also conducted on the complex cavity experimental data. POD modes shapes were similar to the simple rectangular cavity, however, the energy distribution among the mode shapes was different. The complex cavity energy was more widely distributed among the modes, indicated a more complex flow structure. In the future, both the POD and DMD analysis will be applied to computations of the complex cavity. This should better reveal the three-dimensional structure of the flowfield, similar to what has been presented for the simple rectangular cavity.

Acknowledgments

The authors thank Justin Wagner, Steven Beresh, and Matthew Barone for helpful discussions on cavity dynamics. Tom Grasser designed and oversaw construction of the complex geometry hardware.

References

[1]Rockwell, D. and Naudascher, E., "Review-Self-Sustaining Oscillations of Flow Past Cavities," *Journal of Fluids Engineering*, Vol. 100, No. 2, 1978, pp. 152–165.

[2]Rowley, C. W. and Williams, D. R., "Dynamics and Control of High-Reynolds-Number Flow over Open Cavities," *Annual Review of Fluid Mechanics*, Vol. 38, 2006, pp. 251–276.

[3]Rossiter, J. E., "Wind-Tunnel Experiments on the Flow over Rectangular Cavities at Subsonic and Transonic Speeds," Reports & Memoranda 3438, Aeronautical Research Council, October 1964.

[4]Tracy, M. B. and Plentovich, E. B., "Cavity Unsteady-Pressure Measurements at Subsonic and Transonic Speeds," NASA Technical Paper 3669, December 1997.

[5]Dix, R. E. and Bauer, R. C., "Experimental and Theoretical Study of Cavity Acoustics," Tech. Rep. AEDC-TR-99-4, Arnold Engineering Development Center, May 2000.

[6]Heller, H. H. and Bliss, D. B., "The Physical Mechanism for Flow-Induced Pressure Fluctuations in Cavities and Concepts for their Suppression," AIAA Paper 75-491, March 1975.

[7]Wagner, J. L., Casper, K. M., Beresh, S. J., Hunter, P. S., Spillers, R. W., Henfling, J. F., and Mayes, R. L., "Experimental Investigation of Fluid-Structure Interactions in Compressible Cavity Flows," AIAA Paper 2013-3172, June 2013.

[8]Wagner, J. L., Beresh, S. J., Casper, K. M., Henfling, J. F., Spillers, R. W., Hunter, P. S., Blecke, J. C., and Mayes, R. L., "Simultaneous Vibration and Acoustic Measurements of a Store in Compressible Open Cavity Flow," AIAA Paper 2013-0228, January 2013.

[9]Beresh, S. J., Wagner, J. L., Pruett, B. O. M., Henfling, J. F., and Spillers, R. W., "Supersonic Flow over a Finite-Width Rectangular Cavity," *AIAA Journal*, 2014, early edition.

[10]Kannepalli, C., Chartrand, C., Birkbeck, R., Sinha, N., and Murray, N., "Computational Modeling of Geometrically Complex Weapons Bays," AIAA Paper 2011-2774, June 2011.

[11]Bartel, H. W. and McAvoy, J. M., "Cavity Oscillation in Cruise Missile Carrier Aircraft," Tech. Rep. AFWAL-TR-81-3036, Air Force Wright Aeronautical Laboratories, June 1981.

[12]Shaw, L., Clark, R., and Talmadge, D., "F-111 Generic Weapons Bay Acoustic Environment," AIAA Paper 87-0168, January 1987.

[13]Ukeiley, L., Sheehan, M., Coiffet, F., Alvi, F., Arunajatesan, S., and Jansen, B. J., "Control of Pressure Loads in Geometrically Complex Cavities," *Journal of Aircraft*, Vol. 45, No. 3, May–June 2008, pp. 1014–1024.

[14]Tracy, M. B., Plentovich, E. B., Hemsch, M. J., and Wilcox, F. J., "Effect of Sweep on Cavity Flow Fields at Subsonic and Transonic Speeds," Tech. Rep. NASA TM 2012-217577, NASA Langley Research Center, May 2012.

[15]Casper, K. M., Wagner, J. L., Beresh, S. J., Henfling, J. F., Spillers, R. W., and Pruett, B. O. M., "Complex Geometry Effects on Supersonic Cavity Flows," AIAA Paper 2014-3025, June 2014.

[16]Casper, K. M., Wagner, J. L., Beresh, S. J., Henfling, J. F., Spillers, R. W., and Pruett, B. O. M., "Complex Geometry Effects on Subsonic Cavity Flows," AIAA Paper, to appear, January 2015.

[17]Lumley, J. L., *Stochastic Tools in Turbulence*, Academic Press, 1970.

[18]Schmid, P. J., "Dynamic Mode Decomposition of Numerical and Experimental Data," *Journal of Fluid Mechanics*, Vol. 656, 2010, pp. 5–28.

[19]Murray, N., Sällström, E., and Ukeiley, L., "Properties of Subsonic Open Cavity Flow Fields," *Physics of Fluids*, Vol. 29, 2009, pp. 1–16, 095103.

[20]Seena, A. and Sung, H., "Dynamic Mode Decomposition of Turbulent Cavity Flows for Self-Sustained Oscillations," *International Journal of Heat and Fluid Flow*, Vol. 32, October 2011, pp. 1098–1110.

[21]Seena, A. and Sung, H., "Spatiotemporal Representation of the Dynamic Modes in Turbulent Cavity Flows," *International Journal of Heat and Fluid Flow*, Vol. 44, March 2013, pp. 1–11.

[22]Wagner, J. L., Casper, K. M., Beresh, S. J., Henfling, J. F., Spillers, R. W., and Pruett, B. O. M., "Mitigation of Wind Tunnel Wall Interactions in Subsonic Cavity Flows," AIAA Paper 2014-3026, June 2014.

[23]Arunajatesan, S., Bhardwaj, M., Riley, W. C., and Ross, M., "One-Way Coupled Fluid Structure Simulations of Stores in Weapons Bays," AIAA Paper 2013-0665, January 2013.

[24]Arunajatesan, S., Ross, M., Barone, M., and Garret, T. J., "Validation of an FSI Modeling Framework for Internal Captive Carriage Applications," AIAA Paper 2013-2157, June 2013.

[25]Barone, M., Arunajatesan, S., and Chartrand, C., "Features within Geometrically Complex Cavities," AIAA Paper, to appear, June 2015.

[26]Tu, J. H., *Dynamic Mode Decomposition: Theory and Applications*, Ph.D. Thesis, Princeton University, September 2013.

[27]Chatterjee, A., "An Introduction to the Proper Orthogonal Decomposition," *Current Science*, Vol. 78, No. 7, April 2000, pp. 808–817.

[28]Hemati, M., Williams, M., and Rowley, C., "Dynamic Mode Decomposition for Large and Streaming Datasets," *Physics of Fluids*, Vol. 26, 111701, 2014.

[29]Shaikh, F. N. and Gaster, M., "The Non-Linear Evolution of Modulated Waves in a Boundary Layer," *Journal of Engineering Mathematics*, Vol. 28, 1994, pp. 55–71.

[30]Jordan, D., Miksad, R. W., and Powers, E. J., "Implementation of the Continuous Wavelet Transform for Digital Time Series Analysis," *Review of Scientific Instruments*, Vol. 68, No. 3, March 1997, pp. 1484–1494.

[31]Torrence, C. and Compo, G. P., "A Practical Guide to Wavelet Analysis," *Bulletin of the American Meteorological Society*, Vol. 79, No. 1, 1998, pp. 61–78.

[32]Kegerise, M.A. amd Spina, E. F., Garg, S., and Cattafesta, L. N., "Mode-Switching and Nonlinear Effects in Compressible Flow Over a Cavity," *Physics of Fluids*, Vol. 16, No. 3, March 2004, pp. 678–687.